Eur. Phys. J. C (2023) 83:1073
https://doi.org/10.1140/epjc/s10052-023-12235-x

THE EUROPEAN PHYSICAL JOURNAL C

Regular Article - Theoretical Physics

New dark matter candidate in the $B-L$ symmetric SSM

Jin-Lei Yang[1,2,a], **Zhong-Jun Yang**[3,b], **Xiu-Yi Yang**[4,c], **Hai-Bin Zhang**[1,2,d], **Tai-Fu Feng**[1,2,e]

[1] Department of Physics, Hebei University, Baoding 071002, China
[2] Key Laboratory of High-precision Computation and Application of Quantum Field Theory of Hebei Province, Baoding 071002, China
[3] Department of Physics, Chongqing Key Laboratory for Strongly Coupled Physics, Chongqing University, Chongqing 401331, China
[4] Department of Science, University of Science and Technology Liaoning, Anshan 114051, China

Received: 7 June 2023 / Accepted: 6 November 2023 / Published online: 24 November 2023

Abstract The B-L symmetric SUSY model (B-LSSM) introduces a new Z' gauge boson and two singlet scalars, which indicates there are more neutralinos in the B-LSSM comparing with the minimal SUSY extension of standard model (MSSM). These new neutralinos provide more dark matter (DM) candidates in the B-LSSM, we find that the super partner of the new scalar singlet can serve as the lightest supersymmetric particle (LSP) and be considered as a DM candidate. The properties of this new DM candidate are analyzed in this work. Taking into account the experimental constraints on Higgs boson mass, B meson rare decays and muon anomalous magnetic dipole moment, the numerical results are obtained and presented. The properties of new DM candidate in the B-LSSM satisfy the observed relic density Ωh^2 and comply with the latest upper bounds on $\sigma_{\rm SI}^{\chi_1^0-n}$, and its mass is expected to greater than 80 GeV approximately.

1 Introduction

Observations of galaxy rotation curves indicate that the circular velocity remains constant as the radius r increases [1]. This suggests the presence of a halo with mass distribution $M(r) \propto r$ in galaxies. The halo is constructed by invisible matter known as dark matter (DM), which contributes approximately five times more than visible matter as confirmed by the analysis of the cosmic microwave background (CMB) [2,3]. The properties of DM indicate that it must be electrically neutral, color neutral, long-lived and only involved in weak interactions [4,5]. In the standard model (SM), the only potential DM candidates are the neutrinos, but neutrinos in the SM are massless, hence new physics (NP) beyond the SM is required to provide reasonable DM candidates. Furthermore, the relic density of tiny but nonzero massive neutrinos which account for neutrino oscillation experiments, is significantly lower than the relic density of non-baryonic matter $\Omega h^2 = 0.1186 \pm 0.002$ [6,7]. This underscores the need for new DM candidates beyond the SM. Based on current observations, the DM candidate can take the form of either scalar or fermion. Among the various DM candidates, weakly interacting massive particles (WIMPs) are particularly popular [8], as they have the potential to be observed in direct detection experiments [9–13], indirect detection experiments [14,15], and collider experiments [16–18].

The lightest neutralino in supersymmetry (SUSY) models is one of the most attractive candidates for WIMP dark matter (DM). It is electrically neutral, color neutral, long-lived, and serves as an ideal cold DM candidate. In the minimal SUSY extension of the SM (MSSM), the relic density and detection potential of the lightest neutralino as a DM candidate are analyzed in references [19–27]. These analyses demonstrate that the parameter space of the MSSM is strongly constrained when considering collider, astrophysics and muon anomalous magnetic dipole moment (MDM) constraints. Therefore, the DM sector coupled with the existence of nonzero neutrino masses, call for the consideration of an extended SUSY scenario. We focus on analyzing the properties of new DM candidates in the $B-L$ symmetric SUSY model (B-LSSM), where B represents the baryon number and L represents the lepton number [28–33]. In comparison to the MSSM, there are more neutralinos in the B-LSSM, which indicates a larger pool of potential DM candidates.

[a] e-mail: jlyang@hbu.edu.cn (corresponding author)
[b] e-mail: zj_yang@cqu.edu.cn
[c] e-mail: yxyruxi@163.com
[d] e-mail: hbzhang@hbu.edu.cn
[e] e-mail: fengtf@hbu.edu.cn

The local gauge group of the B-LSSM is extended as $SU(3)_C \otimes SU(2)_L \otimes U(1)_Y \otimes U(1)_{B-L}$, the invariance under $U(1)_{B-L}$ gauge group imposes the R-parity conservation which is assumed in the MSSM to avoid proton decay. And R-parity conservation can be maintained if $U(1)_{B-L}$ symmetry is broken spontaneously [34]. Three right-handed neutrinos and two singlet scalars with nonzero $B-L$ charge are introduced in the B-LSSM. The tiny neutrino masses can be acquired naturally by the so-called type-I seesaw mechanism when the introduced singlet scalars receive vacuum expect values (VEVs) after the symmetry breaking. As can be noted, there are three additional neutralinos in the B-LSSM comparing with the MSSM, which are the supper partners of two singlet scalars and a new Z' gauge boson. These new neutralinos have the potential to serve as DM candidates. In this study, we analyze the properties of these newly proposed DM candidates in the B-LSSM, and investigate whether their relic density and cross sections with nucleon align with the experimental measurements. It is widely acknowledged that the relic density of Bino, Wino, or Higgsino DM candidates in the MSSM is hard to match experimental measurements when considering muon anomalous MDM constraints. Therefore, we incorporate the observed muon anomalous MDM constraints in our analysis.

The paper is organized as follows. Section 2 presents the framework of the B-LSSM, the neutralino mass matrix, the relic density of the DM candidate, and the cross section of DM candidates scattering with nucleons. The numerical results are calculated and analyzed in Sect. 3. Finally, a brief summary is given in Sect. 4.

2 The new DM candidates in the B-LSSM

This section presents the framework of the B-LSSM, calculates the relic density for potential DM candidate and the cross section of DM candidate scattering with nucleon.

2.1 The B-LSSM

The gauge group of B-LSSM is extended to include an additional $U(1)_{B-L}$ local gauge group, which results in the introduction of a new Z' gauge boson. In addition, three generations of right-handed neutrinos $\hat{\nu}_R \sim (1,1,0,1/2)$ and two chiral singlet superfields $\hat{\eta}_1 \sim (1,1,0,-1)$, $\hat{\eta}_2 \sim (1,1,0,1)$ are introduced, and the superpotential is given by

$$\begin{aligned} W = & Y_u^{ij}\hat{Q}_i\hat{H}_2\hat{U}_j^c + \mu H_1 H_2 - Y_d^{ij}\hat{Q}_i\hat{H}_1\hat{D}_j^c - Y_e^{ij}\hat{L}_i\hat{H}_1\hat{E}_j^c \\ & + Y_\nu^{ij}\hat{L}_i\hat{H}_2\hat{\nu}_{R,j} - \mu'\hat{\eta}_1\hat{\eta}_2 + Y_x^{ij}\nu_{R,i}\hat{\eta}_1\nu_{R,j}. \end{aligned} \tag{1}$$

The right-handed neutrinos acquire Majorana masses as the two singlet scalars receive VEVs $u_1,\ u_2$ after the symmetry breaking

$$\begin{aligned} \eta_1 &= \frac{1}{\sqrt{2}}(u_1 + \mathrm{Re}\eta_1 + i\mathrm{Im}\eta_1), \\ \eta_2 &= \frac{1}{\sqrt{2}}(u_2 + \mathrm{Re}\eta_2 + i\mathrm{Im}\eta_2). \end{aligned} \tag{2}$$

Combining with the Dirac mass terms acquired after the two doublet scalars

$$\begin{aligned} H_1 &= \begin{pmatrix} H_1^1 \\ H_1^2 \end{pmatrix} \sim (1,2,-1/2,0), \\ H_2 &= \begin{pmatrix} H_2^1 \\ H_2^2 \end{pmatrix} \sim (1,2,1/2,0) \end{aligned} \tag{3}$$

receive VEVs $v_1,\ v_2$

$$\begin{aligned} H_1^1 &= \frac{1}{\sqrt{2}}(v_1 + \mathrm{Re}H_1^1 + i\mathrm{Im}H_1^1), \\ H_2^2 &= \frac{1}{\sqrt{2}}(v_2 + \mathrm{Re}H_2^2 + i\mathrm{Im}H_2^2), \end{aligned} \tag{4}$$

the observed tiny neutrino masses can be obtained by the so-called type I see-saw mechanism in the B-LSSM. For convenience, we can define $v^2 = v_1^2 + v_2^2$, $u^2 = u_1^2 + u_2^2$, $\tan\beta = v_2/v_1$, $\tan\beta' = u_2/u_1$, and the new Z' gauge boson mass can be approximated as $M_{Z'} \approx g_B u$ where g_B is the gauge coupling constant corresponding to $U(1)_{B-L}$. The soft breaking terms of the model can be written as

$$\begin{aligned} \mathcal{L}_{\mathrm{soft}} = & \Big[-\frac{1}{2}(M_1\tilde{\lambda}_B\tilde{\lambda}_B + M_2\tilde{\lambda}_W\tilde{\lambda}_W + M_3\tilde{\lambda}_g\tilde{\lambda}_g \\ & + 2M_{BB'}\tilde{\lambda}_{B'}\tilde{\lambda}_B + M_{B'}\tilde{\lambda}_{B'}\tilde{\lambda}_{B'}) \\ & - B_\mu H_1 H_2 - B_{\mu'}\tilde{\eta}_1\tilde{\eta}_2 + T_{u,ij}\tilde{Q}_i\tilde{u}_j^c H_2 \\ & + T_{d,ij}\tilde{Q}_i\tilde{d}_j^c H_1 + T_{e,ij}\tilde{L}_i\tilde{e}_j^c H_1 + T_\nu^{ij} H_2\tilde{\nu}_i^c\tilde{L}_j \\ & + T_x^{ij}\tilde{\eta}_1\tilde{\nu}_i^c\tilde{\nu}_j^c + h.c.\Big] - m^2_{\tilde{\nu},ij}(\tilde{\nu}_i^c)^*\tilde{\nu}_j^c \\ & - m^2_{\tilde{q},ij}\tilde{Q}_i^*\tilde{Q}_j - m^2_{\tilde{u},ij}(\tilde{u}_i^c)^*\tilde{u}_j^c - m^2_{\tilde{\eta}_1}|\tilde{\eta}_1|^2 \\ & - m^2_{\tilde{\eta}_2}|\tilde{\eta}_2|^2 - m^2_{\tilde{d},ij}(\tilde{d}_i^c)^*\tilde{d}_j^c - m^2_{\tilde{L},ij}\tilde{L}_i^*\tilde{L}_j \\ & - m^2_{\tilde{e},ij}(\tilde{e}_i^c)^*\tilde{e}_j^c - m^2_{H_1}|H_1|^2 - m^2_{H_2}|H_2|^2, \end{aligned} \tag{5}$$

with $\lambda_B, \lambda_{B'}$ denoting the gaugino of $U(1)_Y$ and $U(1)_{B-L}$ respectively.

It is worth noting that the B-LSSM introduces three additional neutralinos, which correspond to the super partners of two singlet scalars and a new Z' gauge boson. These neutralinos have the potential to serve as cold DM candidates. On the basis $(\tilde{\lambda}_B, \tilde{\lambda}_W, \tilde{\lambda}_{H_1^1}, \tilde{\lambda}_{H_2^2}, \tilde{\lambda}_{B'}, \tilde{\lambda}_{\eta_1}, \tilde{\lambda}_{\eta_2})$, the mass matrix of neutralinos in the B-LSSM can be written as

$$M_{\chi^0} = \begin{pmatrix} M_1 & 0 & -\frac{1}{2}g_1v_1 & \frac{1}{2}g_1v_2 & M_{BB'} & 0 & 0 \\ 0 & M_2 & \frac{1}{2}g_2v_1 & -\frac{1}{2}g_2v_2 & 0 & 0 & 0 \\ -\frac{1}{2}g_1v_1 & \frac{1}{2}g_2v_1 & 0 & -\mu & -\frac{1}{2}g_{YB}v_1 & 0 & 0 \\ \frac{1}{2}g_1v_2 & -\frac{1}{2}g_2v_2 & -\mu & 0 & \frac{1}{2}g_{YB}v_2 & 0 & 0 \\ M_{BB'} & 0 & -\frac{1}{2}g_{YB}v_1 & \frac{1}{2}g_{YB}v_2 & M_{BL} & -g_Bu_1 & g_Bu_2 \\ 0 & 0 & 0 & 0 & -g_Bu_1 & 0 & -\mu' \\ 0 & 0 & 0 & 0 & g_Bu_2 & -\mu' & 0 \end{pmatrix}, \tag{6}$$

where g_{YB} is the gauge coupling constant arising from the gauge kinetic mixing effects in the models with two Abelian gauge groups. For gaugino mass terms M_1, M_2, μ appeared in Eq. (6), we take $M_0 \equiv \mu = 2M_1 = 2M_2$ in the following analysis for simplicity. In order to obtain the analytical masses of the additional neutralinos approximately, we neglect the mixing effects between the MSSM sector with the B-LSSM sector in Eq. (6), i.e. we take $M_{BB'} = 0$, $g_{YB} = 0$ and $M_{BL} \ll u$, $\mu_B \ll u$. Under these assumptions, the masses corresponding to $\tilde{\lambda}_{B'}, \tilde{\lambda}_{\eta_1}, \tilde{\lambda}_{\eta_2}$ can be expressed as:

$$\begin{aligned} M_{\chi^0_{\tilde{B}'}} &\approx M_{Z'} + \frac{1}{2}M_{BL} + \frac{\tan\beta'}{\tan^2\beta'+1}\mu_B, \\ M_{\chi^0_{\tilde{\eta}_1}} &\approx \frac{2\tan\beta'}{\tan^2\beta'+1}\mu_B, \\ M_{\chi^0_{\tilde{\eta}_2}} &\approx M_{Z'} - \frac{1}{2}M_{BL} - \frac{\tan\beta'}{\tan^2\beta'+1}\mu_B. \end{aligned} \tag{7}$$

The updated experimental data on searching Z' gauge boson shows $M_{Z'} > 4.05$ TeV at 95% confidence level [35]. And Eq. (7) indicates that the super partners of Z' gauge boson and η_2 is significantly heavy and unlikely to serve as the LSP for potential dark matter candidates.[1] However, $M_{\chi^0_{\tilde{\eta}_1}}$ is equal to μ_B approximately and can be considered as a potential DM candidate in the B-LSSM. Therefore, we focus on $\chi^0_{\tilde{\eta}_1}$, the super partner of η_1, as the DM candidate in the B-LSSM and investigate its relic density and scattering cross section with nucleon to see weather it can satisfy the experimental observations. For simplicity, the neutralinos in the B-LSSM are denoted by χ^0_i, $(i = 1, ..., 7)$ in the following analysis, and the corresponding masses have $M_{\chi^0_i} < M_{\chi^0_j}$ when $i < j$.

The co-annihilation processes involving charginos should be considered in the calculations of DM relic density. The chargino sector in the B-LSSM is same as the one in the MSSM, and the corresponding mass matrix can be written as

$$M_{\chi^\pm} = \begin{pmatrix} M_2, & \frac{1}{\sqrt{2}}g_2v_2 \\ \frac{1}{\sqrt{2}}g_2v_1, & \mu \end{pmatrix}. \tag{8}$$

2.2 The relic density and direct detection of DM

We adopt the methods described in Ref. [36] to determine the relic density of DM. The abundances of new particles χ_i $(i = 1, ..., N)$ beyond the SM with $m_i < m_j$ for $i < j$ are determined by the Boltzmann equations

$$\begin{aligned} \frac{dn_i}{dt} = &-3Hn_i - \sum_{j,X}[\langle\sigma_{ij}v\rangle(n_in_j - n_i^{\rm eq}n_j^{\rm eq}) \\ &-(\langle\sigma'_{ij}v\rangle n_in_X - \langle\sigma'_{ji}v\rangle n_jn_X) \\ &-\Gamma_{ij}(n_i - n_i^{\rm eq})], \end{aligned} \tag{9}$$

where H is the Hubble parameter, $n_i^{\rm eq}$ is the χ_i equilibrium number density, v is the "relative velocity", $\langle\sigma_{ij}v\rangle$ is the thermal average of the corresponding annihilation cross section which can be Taylor expanded as $\langle\sigma_{ij}v\rangle = a_{ij} + b_{ij}\langle v^2\rangle$, and

$$\begin{aligned} \sigma_{ij} &= \sigma(\chi_i\chi_j \to XX'), \\ \sigma'_{ij} &= \sigma(\chi_iX \to \chi_jX'), \\ \Gamma_{ij} &= \sigma(\chi_i \to \chi_jXX'). \end{aligned} \tag{10}$$

X, X' denote the SM particles. The Boltzmann equation determining the abundance of DM can be obtained from Eq. (9) as

$$\frac{dn}{dt} = -3Hn - \sum_{i=1,j=1}^{N}[\langle\sigma_{ij}v\rangle(n_in_j - n_i^{\rm eq}n_j^{\rm eq})]. \tag{11}$$

where $n = \sum_{i=1}^{N} n_i$ because all χ_i which survive annihilation eventually decay into the LSP χ_1. Defining

$$\begin{aligned} r_i &= n_i^{\rm eq}/n^{\rm eq} = \frac{g_i(1+\Delta_i)^{3/2}e^{-x\Delta_i}}{g_{\rm eff}}, \\ \Delta_i &= (m_i - m_1)/m_1, \\ g_{\rm eff} &= \sum_{i=1}^{N} g_i(1+\Delta_i)^{3/2}e^{-x\Delta_i}, \quad x \equiv \frac{m}{T}, \end{aligned} \tag{12}$$

[1] The results in Eq. (7) indicate that $M_{\chi^0_{\tilde{\eta}_2}}$ is possibly small when M_{BL} or μ_B is large. However, the expressions in Eq. (7) are invalid for large M_{BL} or μ_B, because Eq. (7) is obtained under the assumption $M_{BL} \ll u$, $\mu_B \ll u$. And we verify numerically that $M_{\chi^0_{\tilde{\eta}_2}}$ is too heavy to be the LSP even if the cancellations take place in Eq. (7).

where T denotes temperature, g_i is the number of degrees of freedom of χ_i. Equation (11) can be rewritten as

$$\frac{dn}{dt} = -3Hn - \langle\sigma_{\rm eff} v\rangle(n^2 - n_{\rm eq}^2), \tag{13}$$

where

$$\begin{aligned}\sigma_{\rm eff} &= \sum_{ij}^{N} r_i r_j \\ &= \sum_{ij}^{N} \sigma_{ij} \frac{g_i g_j}{g_{\rm eff}} (1+\Delta_i)^{3/2}(1+\Delta_j)^{3/2} e^{-x(\Delta_i+\Delta_j)}.\end{aligned} \tag{14}$$

The DM freeze-out temperature X_F can be obtained by

$$X_F = \ln \frac{0.038 g_{\rm eff} M_{PL} M_{DM} \langle\sigma_{\rm eff} v\rangle}{g_*^{1/2} X_F^{1/2}}, \tag{15}$$

with $M_{\rm DM}$ denoting the DM mass, $M_{PL} = 1.22\times 10^{19}$ GeV, and g_* being the total number of effectively relativistic degrees of freedom at the time of freeze-out. Finally, the relic density of DM χ_1 can be written as

$$\Omega h^2 = \frac{1.07\times 10^9 x_F}{g_\star^{1/2} M_{\rm PL}(a_{11} I_a + 3 b_{11} I_b / x_F)}, \tag{16}$$

where

$$\begin{aligned} I_a &= \frac{x_F}{a_{11}} \int_{x_F}^{\infty} x^{-2} a_{\rm eff} dx, \\ I_b &= \frac{2x_F^2}{a_{11}} \int_{x_F}^{\infty} x^{-3} b_{\rm eff} dx, \end{aligned} \tag{17}$$

and $a_{\rm eff}$ $(b_{\rm eff})$ can be obtained by replacing $\sigma_{\rm eff}$, σ_{ij} in Eq. (14) by $a_{\rm eff}$ $(b_{\rm eff})$, a_{ij} (b_{ij}) respectively.

As analyzed above, the newly possible DM candidate in the B-LSSM is the super partner of the scalar field η_1. The dominant self-annihilation and co-annihilation processes considered in our calculations are

$$\begin{aligned}(1):\ &\chi_j^0\chi_k^0 \to \bar{u}_i u_i,\ \bar{d}_i d_i,\ \bar{l}_i l_i,\ \bar{\nu}_i \nu_i,\ WW,\ ZZ,\ hh,\\ &hZ\ (i=1,2,3,\ j,k=1,2,3),\end{aligned} \tag{18}$$

$$\begin{aligned}(2):\ &\chi_j^0\chi_k^{\pm} \to \bar{u}_i d_i,\ \bar{l}_i \nu_i,\ ZW,\ hW,\\ &rW\ (i=1,2,3,\ j=1,2,3,\ k=1),\end{aligned} \tag{19}$$

$$\begin{aligned}(3):\ &\chi_j^{\pm}\chi_k^{\pm} \to \bar{u}_i u_i,\ \bar{d}_i d_i,\ \bar{l}_i l_i,\ \bar{\nu}_i \nu_i,\ WW,\ ZZ,\ hh,\\ &\gamma\gamma,\ hZ,\ \gamma Z, \gamma h\ (i=1,2,3,\ \ j,k=1).\end{aligned} \tag{20}$$

The results shown in Ref. [37] indicates that the co-annihilation processes involving particle χ_X are highly suppressed when $M_{\chi_X} > 1.5 M_{\rm DM}$, hence we can neglect the contributions from co-annihilation processes to the relic density safely when the involving particles are heavier than $1.5 M_{\chi_1^0}$.

2.3 The direct detection of DM

DM detection experiments set strict constraints on the DM-nucleon scattering cross section, where the most stringent constraints are applied to the spin-independent (SI) scattering. The lower bound on the SI scattering cross section from the LUX-ZEPLIN (LZ) experiments [38] reads 6.5×10^{-48} cm^2 for $M_{\rm DM} = 30$ GeV, while the one reads 2.58×10^{-47} cm^2 for $M_{\rm DM} = 28$ GeV from the recent XENONnT experimental results [39]. The LZ experiments provide the most stringent constraints at present, so we incorporate the constraints derived from the latest LZ experimental results into our analysis.

In the B-LSSM, the effective Lagrangian for SI scattering can be written as

$$\begin{aligned}\mathcal{L}_{SI} &= \left[\frac{(C^L_{\tilde{f}h_i f} + C^R_{\tilde{f}h_i f})(C^L_{\overline{\tilde{\chi}_0^1}h_i\tilde{\chi}_0^1} + C^R_{\overline{\tilde{\chi}_0^1}h_i\tilde{\chi}_0^1})}{-4m_{h_i}^2}\right.\\ &\quad \left. + \frac{C^L_{\tilde{f}\tilde{f}\chi^0} C^R_{\tilde{f}\tilde{f}\chi^0}}{-4m_{\tilde{f}}^2}\right] \overline{\tilde{\chi}_0^1}\tilde{\chi}_0^1 \bar{f} f\\ &\equiv C_{SI}^f \overline{\tilde{\chi}_0^1}\tilde{\chi}_0^1 \bar{f} f,\end{aligned} \tag{21}$$

with f denoting quark, $\tilde{f}$ is the super partner of quark f, and $C_{abc}^{L,R}$ (with a, b, c denoting the interactional particles) are the left-handed, right-handed part of coupling abc respectively. The cross section of DM-nucleon SI scattering is [40]

$$\sigma_{SI}^{\tilde{\chi}_0^1 - n} = \frac{4M^2_{\chi_0^1} m_n^2}{\pi(M_{\chi_0^1} + m_n)^2} |f_n|^2, \tag{22}$$

where m_n is the neuron mass, and [41–43]

$$\begin{aligned} f_n &= \sum_{f=u,d,s} f_{Tf}^n \frac{C_{SI}^f m_n}{m_f}\\ &\quad + \frac{2}{27}\left(1 - \sum_{f=u,d,s} f_{Tf}^n\right) \sum_{f=c,b,t} \frac{C_{SI}^f m_n}{m_f},\\ f_{Tu}^n &= 0.0110,\ \ f_{Tu}^n = 0.0273,\ \ f_{Tu}^n = 0.0447. \end{aligned} \tag{23}$$

3 Numerical results

In this section, we present and analyze the numerical results of the relic density, the cross section of SI scattering with nucleon of new DM candidate in the B-LSSM. As input parameters [6], we take $m_W = 80.385$GeV, $m_Z = 90.1876$GeV, $\alpha_{em}(m_Z) = 1/128.9$, $\alpha_s(m_Z) = 0.118$, the fermion coupling constant $G_F = 1.1664\times 10^{-5}$GeV^{-2}, the lepton masses $m_e = 0.511$ MeV, $m_\mu = 0.105$ GeV, $m_\tau = 1.78$ GeV, the quark masses $m_u = 2.3$ MeV, $m_c = 1.28$ GeV, $m_t = 173.5$ GeV, $m_d = 4.80$ MeV,

$m_s = 0.095$ GeV, $m_b = 4.65$ GeV. The measured Higgs boson mass at 3σ level errors reads [6]

$$m_h = 125.09 \pm 0.72 \text{ GeV}. \tag{24}$$

It is widely recognized that the measured muon anomalous MDM should be taken into account when considering the lightest neutralino as the DM candidate. The experimental average for the deviation between the experimental measurement and SM theoretical prediction of the muon anomalous MDM is given by [44–47]

$$\Delta a_\mu = a_\mu^{\text{exp}} - a_\mu^{\text{SM}} = (25.1 \pm 5.9) \times 10^{-10}. \tag{25}$$

Based on our previous analysis [48,49], the measured muon anomalous MDM prefers the slepton masses are not very heavy than 1.5 TeV approximately, hence we take the three generations of slepton masses equal to 1 TeV for simplicity. For the trilinear Higgs slepton couplings, we define $T_e \equiv \text{diag}(Y_{e_1}, Y_{e_2}, Y_{e_3})A_e$ with $A_e = 0.1$ TeV, where Y_{e_i} $(i = 1, 2, 3)$ is the corresponding Yukawa coupling constant of e_i. In order to coincide with the measured B meson rare decays branching rations [50–52]

$$\begin{aligned} &Br(\bar{B} \to X_s\gamma) = (3.49 \pm 0.19) \times 10^{-4}, \\ &Br(B_s^0 \to \mu^+\mu^-) = (2.9^{+0.7}_{-0.6}) \times 10^{-9}, \end{aligned} \tag{26}$$

we take the charged Higgs mass $M_{H^\pm} = 1.5$ TeV [53], the squark masses are 2 TeV, the trilinear Higgs squark couplings have $T_u \equiv \text{diag}(Y_{u_1}, Y_{u_2}, Y_{u_3})A_q$, $T_d \equiv \text{diag}(Y_{d_1}, Y_{d_2}, Y_{d_3})A_q$ with $A_q = 0.1$ TeV, where Y_{q_i} $(q = u, d, \ i = 1, 2, 3)$ is the corresponding Yukawa coupling constant of q_i.

As mentioned above, $M_{Z'} > 4.05$ TeV with 95% confidence level and we take $M_{Z'} = 5.0$ TeV without losing generality because the contributions from Z' are suppressed by its heavy mass. The new gauge coupling constants g_B, g_{YB} are taken as $g_B = 0.4$, $g_{YB} = -0.4$ in the calculations. All parameters fixed above affect the relic density and cross section scattering with nucleon of the new DM candidate in the B-LSSM negligibly. For the gaugino mass term $M_0 \equiv \mu = 2M_1 = 2M_2$, we take $M_0 = 2(\mu_B + \Delta)$ where Δ reflects the mass differences between $M_{\chi_1^0}$ with $M_{\chi_2^0}$, $M_{\chi_3^0}$ or $M_{\chi_1^\pm}$ directly because $M_{\chi_1^0} \approx \mu_B$, $M_{\chi_2^0} \approx M_1$, $M_{\chi_3^0} \approx M_2$, $M_{\chi_1^\pm} \approx M_2$.

In order to see the effects of μ_B and Δ, we take $M_B = M_{BB'} = 0.5$ TeV, $\tan\beta = 20$, $\tan\beta' = 1.15$ and plot Ωh^2 versus Δ in Fig. 1a, where the solid, dashed, dotted lines denote the results for $\mu_B = 0.1,\ 0.4,\ 0.7$ TeV respectively, the gray area denotes the experimental 3σ interval of Ωh^2. Similarly, the results of SI DM-nucleon scattering cross section $\sigma_{\text{SI}}^{\chi_1^0-n}$ versus Δ are plotted in Fig. 1b, where red solid, red dashed, red dotted lines denote the LZ experimental upper bounds on $\sigma_{\text{SI}}^{\chi_1^0-n}$ for $\mu_B = 0.1,\ 0.4,\ 0.7$ TeV respectively.

Figure 1a shows that Ωh^2 increases quickly with the increasing of Δ, because the self-annihilation cross section of $\chi_{\tilde{\eta}_1}^0$ is small due to its tiny interactions with the SM particles, and the relic density of $\chi_{\tilde{\eta}_1}^0$ depends on the co-annihilation processes dominantly while the cross sections of co-annihilation processes are proportional to $e^{-x(\Delta_i+\Delta_j)}$ as shown in Eq. (14). In addition, Δ is limited strictly by considering Ωh^2 in the experimental 3σ interval for given DM mass (i.e. for given μ_B). It is obvious in Fig. 1b that the obtained $\sigma_{\text{SI}}^{\chi_1^0-n}$ is well below the LZ experimental upper bounds in the considered parameter space. $\sigma_{\text{SI}}^{\chi_1^0-n}$ mainly depends on the DM mass and increases slowly with the increasing of Δ.

In deriving Eq. (7), we set $M_{BB'} = 0$ and make the approximate assumptions $M_{BL} \ll u,\ \mu_B \ll u$. In fact, the new gaugino mass terms $M_{BB'}$, M_{BL} can also influence the mass differences $M_{\chi_2^0} - M_{\chi_1^0}$, thereby affecting the relic density of the new DM candidate $\chi_{\tilde{\eta}_1}^0$. Taking $\tan\beta' = 1.15$, $\tan\beta = 20$, $\mu_B = 0.4$ TeV, $\Delta = 84$ MeV, the results of Ωh^2 versus $M_{BB'}$ are plotted in Fig. 2a, where the gray area denotes the experimental 3σ interval of Ωh^2, the solid, dashed, dotted lines denote the results for $M_{BL} = 0,\ 1,\ 2$ TeV respectively. Similarly, $\sigma_{\text{SI}}^{\chi_1^0-n}$ and $M_{\chi_2^0} - M_{\chi_1^0}$ versus $M_{BB'}$ are plotted in Fig. 2b and c respectively, where the red solid line in Fig. 2b denotes the LZ experimental upper bounds on $\sigma_{\text{SI}}^{\chi_1^0-n}$ for $\mu_B = 0.4$ TeV.

Figure 2a shows that the relic density Ωh^2 initially increases and then decreases with the decreasing of $|M_{BB'}|$. From Fig. 2c, it can be seen that the mass difference $M_{\chi_2^0} - M_{\chi_1^0}$ increases with the decreasing of $|M_{BB'}|$ which leads to the increases of Ωh^2 in Fig. 2a. On the other hand, $|M_{BB'}|$ can also affect the χ_i^0 $(i = 2,\ 3)$ coupling strength with SM particles which leads to the decreasing of Ωh^2 in Fig. 2a when $|M_{BB'}|$ approaches to 0. Figure 2b demonstrates that the SI DM-nucleon scattering cross section $\sigma_{\text{SI}}^{\chi_1^0-n}$ is well below the upper bounds set by the LZ experiments.

As shown in Eq. (6), $\tan\beta$ and $\tan\beta'$ can potentially influence the mass matrix of neutralinos. In order to see the effects of $\tan\beta$, $\tan\beta'$, we take $\mu_B = 0.4$ TeV, $\Delta = 84$ MeV, $M_B = M_{BB'} = 0.5$ TeV and plot Ωh^2, $\sigma_{\text{SI}}^{\chi_1^0-n}$, $M_{\chi_2^0} - M_{\chi_1^0}$ versus $\tan\beta'$ in Fig. 3a–c respectively, where the black solid, black dashed, black dotted lines denote the results for $\tan\beta = 10,\ 20,\ 30$ respectively, the gray area in Fig. 3a denotes the experimental 3σ interval of Ωh^2, the red solid line in Fig. 3b denotes the LZ experimental upper bounds on $\sigma_{\text{SI}}^{\chi_1^0-n}$ for $\mu_B = 0.4$ TeV.

To maintain consistency with the experimental 3σ interval of the Higgs boson mass in the B-LSSM, we consider $\tan\beta' \geq 1.1$ in the plotting. Figure 3a clearly demonstrates that the relic density Ωh^2 increases quickly with the increas-

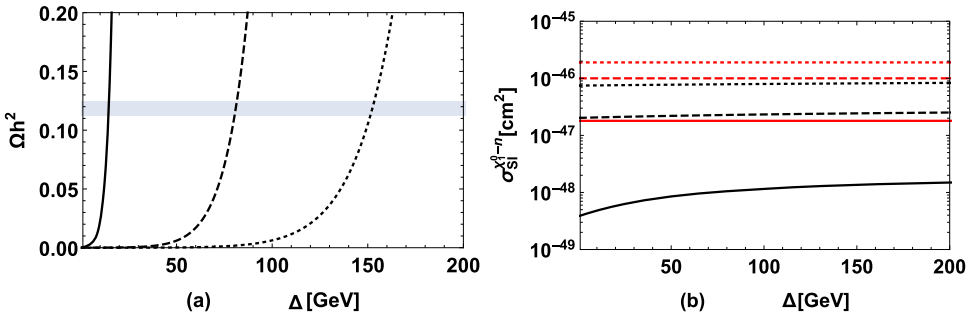

Fig. 1 Taking $M_B = M_{BB'} = 0.5$ TeV, $\tan\beta = 20$ and $\tan\beta' = 1.15$, Ωh^2 (**a**) and $\sigma_{\rm SI}^{\chi_1^0-n}$ (**b**) versus Δ are plotted, where the black solid, black dashed, black dotted lines denote the results for $\mu_B = 0.1,\ 0.4,\ 0.7$ TeV respectively, the gray area in **a** denotes the experimental 3σ interval of Ωh^2, the red solid, red dashed, red dotted lines in **b** denote the LZ experimental upper bounds on $\sigma_{\rm SI}^{\chi_1^0-n}$ for $\mu_B = 0.1,\ 0.4,\ 0.7$ TeV respectively

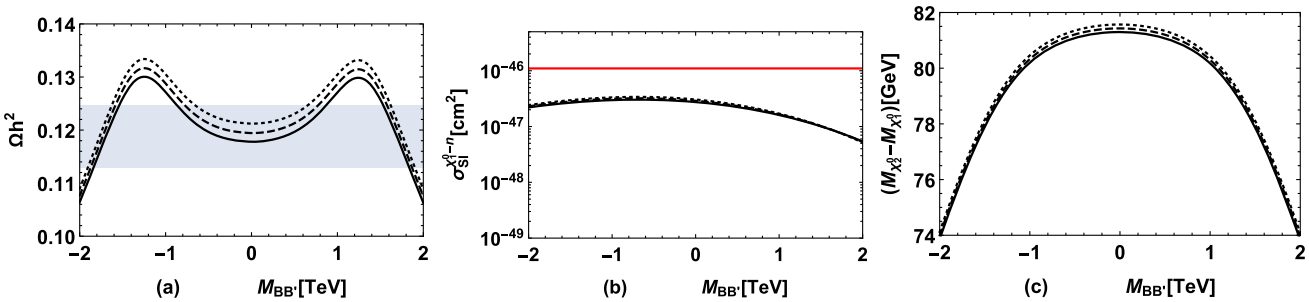

Fig. 2 Taking $\tan\beta' = 1.15$, $\tan\beta = 20$, $\mu_B = 0.4$ TeV, $\Delta = 84$ MeV, Ωh^2 (**a**), $\sigma_{\rm SI}^{\chi_1^0-n}$ (**b**) and $M_{\chi_2^0} - M_{\chi_1^0}$ (**c**) versus $M_{BB'}$ are plotted, where the black solid, black dashed, black dotted lines denote the results for $M_{BL} = 0,\ 1,\ 2$ TeV respectively, the gray area in **a** denotes the experimental 3σ interval of Ωh^2, the red solid line in **b** denotes the LZ experimental upper bounds on $\sigma_{\rm SI}^{\chi_1^0-n}$ for $\mu_B = 0.4$ TeV

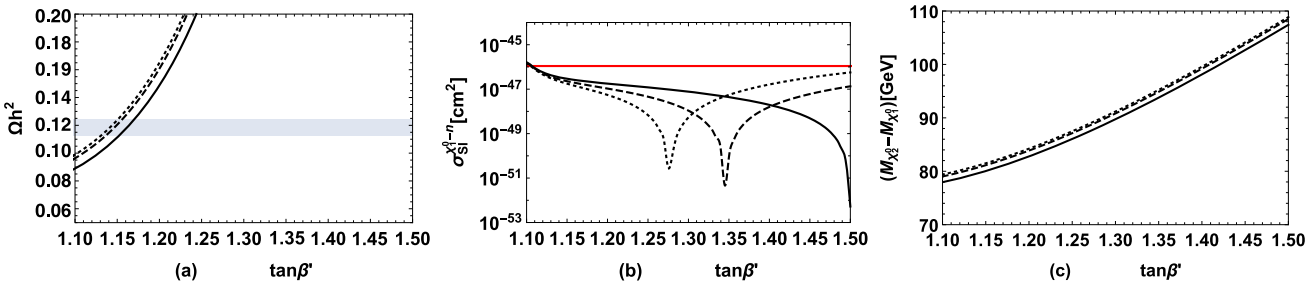

Fig. 3 Taking $M_B = M_{BB'} = 0.5$ TeV, $\mu_B = 0.4$ TeV, $\Delta = 84$ MeV, Ωh^2 (**a**), $\sigma_{\rm SI}^{\chi_1^0-n}$ (**b**) and $M_{\chi_2^0} - M_{\chi_1^0}$ (**c**) versus $\tan\beta'$ are plotted, where the black solid, black dashed, black dotted lines denote the results for $\tan\beta = 10,\ 20,\ 30$ respectively, the gray area in **a** denotes the experimental 3σ interval of Ωh^2, the red solid line in **b** denotes the LZ experimental upper bounds on $\sigma_{\rm SI}^{\chi_1^0-n}$ for $\mu_B = 0.4$ TeV

ing of $\tan\beta'$, owing to the simultaneous increase in the mass difference $M_{\chi_2^0} - M_{\chi_1^0}$ as shown in Fig. 3c. In addition, from Fig. 3a, c we can see that $\tan\beta$ affects relic density Ωh^2 and the mass difference $M_{\chi_2^0} - M_{\chi_1^0}$ mildly. Figure 3b shows that with the increasing of $\tan\beta'$, the DM-nucleon SI scattering cross section $\sigma_{\rm SI}^{\chi_1^0-n}$ decreases to a minimum value and then increases. The specific value of $\tan\beta'$ at which $\sigma_{\rm SI}^{\chi_1^0-n}$ starts to increase depends on the chosen value of $\tan\beta$. And $\sigma_{\rm SI}^{\chi_1^0-n}$ is beyond the LZ experimental upper bound in our chosen parameter space when $\tan\beta' \lesssim 1.107$.

To investigate the combined effects of $\tan\beta$, $\tan\beta'$, μ_B, M_{BL}, $M_{BB'}$ and Δ, we scan the following parameter space

$$\tan\beta = (5, 40),\ \tan\beta' = (1.05, 1.5),$$
$$\mu_B = (0.01, 1.0)\ \text{TeV},\ M_{BL} = (-2, 2)\ \text{TeV},$$

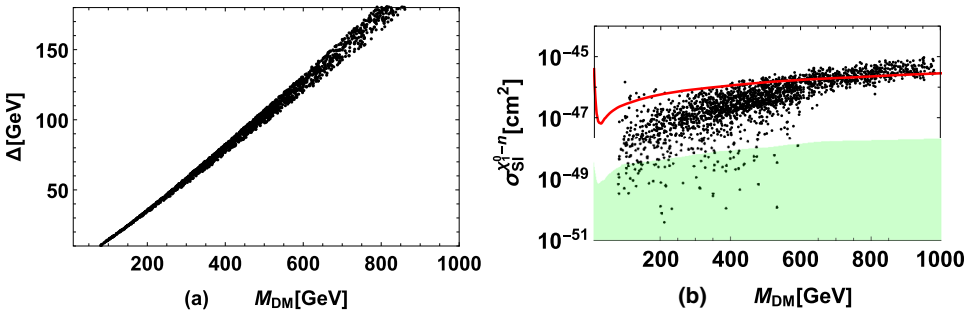

Fig. 4 Scanning the parameter space in Eq. (27) and keeping the muon anomalous MDM, the B meson rare decay branching ratios, the relic density and the Higgs boson mass in their respective experimental 3σ interval, the allowed ranges of Δ, $M_{\rm DM}$ (**a**) and $\sigma_{\rm SI}^{\chi_1^0-n}$ versus $M_{\rm DM}$ (**b**) are plotted, where the red solid line in **b** denotes the LZ experimental upper bounds on $\sigma_{\rm SI}^{\chi_1^0-n}$ the green area denotes the neutrino floor

$$M_{BB'} = (-2, 2)\ \text{TeV},\ \ \Delta = (-0.1, 0.5)\ \text{TeV}, \tag{27}$$

and keep the muon anomalous MDM, the B meson rare decay branching ratios, the relic density and the Higgs boson mass in their respective experimental 3σ interval in the scanning. Then we plot the allowed ranges of Δ, $M_{\rm DM}$ in Fig. 4a. $\sigma_{\rm SI}^{\chi_1^0-n}$ versus $M_{\rm DM}$ is plotted in Fig. 4b, where the red solid line in Fig. 4b denotes the LZ experimental upper bounds on $\sigma_{\rm SI}^{\chi_1^0-n}$ the green area denotes the neutrino floor.

It is evident from the figure that for $\chi_{\tilde{\eta}_1}^0$ to be the dark matter candidate in the B-LSSM, the minimum dark matter mass of approximately 80 GeV is required to satisfy the observed relic density. Furthermore, Fig. 4a illustrates that Δ is limited more strictly for smaller $M_{\rm DM}$, and more points are excluded by the LZ experimental upper bound on $\sigma_{\rm SI}^{\chi_1^0-n}$ as $M_{\rm DM}$ increases which is shown explicitly in Fig. 4b.

4 Summary

In this work, we focus on the potential new DM candidates in the B-LSSM. Comparing with the MSSM, there are three additional neutralinos in the B-LSSM which provide more DM candidates. Considering the experimental lower bound on the Z' gauge boson mass, we find that the super partner of singlet scalar η_1 can be considered as the DM candidate in the B-LSSM. The relic density of $\chi_{\tilde{\eta}_1}^0$ (i.e. χ_1^0) and the SI scattering cross section with nucleon $\sigma_{\rm SI}^{\chi_1^0-n}$ are calculated. Taking into account the experimental constraints from Higgs boson mass, B meson rare decays and muon anomalous MDM, the numerical results are obtained and analyzed. It is found that the properties of new DM candidate $\chi_{\tilde{\eta}_1}^0$ in the B-LSSM satisfy the observed relic density Ωh^2 and comply with the latest upper bounds on $\sigma_{\rm SI}^{\chi_1^0-n}$. The co-annihilation processes play dominant roles on the relic density Ωh^2 which indicates the mass differences between $\chi_{\tilde{\eta}_1}^0$ with the other SUSY particles affect Ωh^2 obviously. The theoretical predictions on Ωh^2 and $\sigma_{\rm SI}^{\chi_1^0-n}$ are also influenced by the new gaugino mass terms M_{BL}, $M_{BB'}$ and new parameters $\tan\beta'$ in the B-LSSM. In addition, for $\chi_{\tilde{\eta}_1}^0$ to be the DM candidate in the B-LSSM, its mass is expected to greater than 80 GeV approximately as shown in Fig. 4.

Acknowledgements The work has been supported by the National Natural Science Foundation of China (NNSFC) with Grants no. 12075074, no. 12235008, no. 11535002, no. 11705045, Hebei Natural Science Foundation for Distinguished Young Scholars with Grant no. A2022201017, Natural Science Foundation of Guangxi Autonomous Region with Grant no. 2022GXNSFDA035068, and the youth top-notch talent support program of the Hebei Province.

Data Availability Statement This manuscript has associated data in a data repository. [Authors' comment: All data included in this manuscript are available upon request by contacting with the corresponding author.]

Funded by SCOAP^3. SCOAP^3 supports the goals of the International Year of Basic Sciences for Sustainable Development.

References

1. K.G. Begeman, A.H. Broeils, R.H. Sanders, Mon. Not. R. Astron. Soc. **249**, 523 (1991)
2. R.H. Cyburt, Phys. Rev. D **70**, 023505 (2004)
3. P.A.R. Ade et al., Planck, Astron. Astrophys. **571**, A31 (2014)
4. M. Drees, M.M. Nojiri, Phys. Rev. D **47**, 376–408 (1993)
5. L.B. Jia, Eur. Phys. J. C **79**(1), 80 (2019)

6. R.L. Workman et al., [Particle Data Group], PTEP **2022**, 083C01 (2022)
7. P.A.R. Ade et al., Planck, Astron. Astrophys. **594**, A13 (2016)
8. G. Arcadi, M. Dutra, P. Ghosh, M. Lindner, Y. Mambrini, M. Pierre, S. Profumo, F.S. Queiroz, Eur. Phys. J. C **78**(3), 203 (2018)
9. D.S. Akerib et al., [LUX], Phys. Rev. Lett. **116**(16), 161302 (2016)
10. E. Aprile et al., XENON, JCAP **04**, 027 (2016)
11. P.L. Brink et al., [CDMS-II], eConf **C041213**, 2529 (2004)
12. T. Tanaka et al., Super-Kamiokande, Astrophys. J. **742**, 78 (2011)
13. R. Abbasi et al., IceCube, Phys. Rev. Lett. **102**, 201302 (2009)
14. W.B. Atwood et al., Fermi-LAT, Astrophys. J. **697**, 1071–1102 (2009)
15. H. Abdallah et al., [H.E.S.S.], Phys. Rev. Lett. **117**(11), 111301 (2016)
16. O. Buchmueller, C. Doglioni, L.T. Wang, Nat. Phys. **13**(3), 217–223 (2017)
17. A. Basalaev [ATLAS], EPJ Web Conf. **164**, 08008 (2017)
18. S. Chatrchyan et al., CMS, JHEP **09**, 094 (2012)
19. M. Beneke, A. Bharucha, F. Dighera, C. Hellmann, A. Hryczuk, S. Recksiegel, P. Ruiz-Femenia, JHEP **03**, 119 (2016)
20. M.E. Cabrera, J.A. Casas, A. Delgado, S. Robles, R. Ruiz de Austri, JHEP **08**, 058 (2016)
21. A. Hebbar, Q. Shafi, C.S. Un, Phys. Rev. D **95**(11), 115026 (2017)
22. M. Chakraborti, U. Chattopadhyay, S. Poddar, JHEP **09**, 064 (2017)
23. W. Ahmed, L. Calibbi, T. Li, S. Raza, J.S. Niu, X.C. Wang, JHEP **06**, 126 (2018)
24. M. Abdughani, K.I. Hikasa, L. Wu, J.M. Yang, J. Zhao, JHEP **11**, 095 (2019)
25. C. Borschensky, G. Coniglio, B. Jäger, Eur. Phys. J. C **79**(5), 428 (2019)
26. P. Cox, C. Han, T.T. Yanagida, Phys. Rev. D **104**(7), 075035 (2021)
27. J.L. Evans, K.A. Olive, Phys. Rev. D **106**(5), 055026 (2022)
28. S. Khalil, H. Okada, Phys. Rev. D **79**, 083510 (2009)
29. A. Elsayed, S. Khalil, S. Moretti, Phys. Lett. B **715**, 208–213 (2012)
30. A. Elsayed, S. Khalil, S. Moretti, A. Moursy, Phys. Rev. D **87**(5), 053010 (2013)
31. W. Abdallah, A. Hammad, S. Khalil, S. Moretti, Phys. Rev. D **95**(5), 055019 (2017)
32. S. Khalil, S. Moretti, Rep. Prog. Phys. **80**(3), 036201 (2017)
33. L. Delle Rose, S. Khalil, S.J.D. King, S. Kulkarni, C. Marzo, S. Moretti, C.S. Un, JHEP **07**, 100 (2018)
34. C.S. Aulakh, A. Melfo, A. Rasin, G. Senjanovic, Phys. Lett. B **459**, 557–562 (1999)
35. ATLAS Collaboration, Report No. ATLAS-CONF-2016-045
36. K. Griest, D. Seckel, Phys. Rev. D **43**, 3191–3203 (1991)
37. J. Edsjo, M. Schelke, P. Ullio, P. Gondolo, JCAP **04**, 001 (2003)
38. J. Aalbers et al., [LZ], arXiv:2207.03764 [hep-ex]
39. E. Aprile et al. [XENON], arXiv:2303.14729 [hep-ex]
40. M. Freytsis, Z. Ligeti, Phys. Rev. D **83**, 115009 (2011)
41. T. Bringmann, J. Edsjö, P. Gondolo, P. Ullio, L. Bergström, JCAP **07**, 033 (2018)
42. G. Bélanger, F. Boudjema, A. Goudelis, A. Pukhov, B. Zaldivar, Comput. Phys. Commun. **231**, 173–186 (2018)
43. W. Chao, JHEP **11**, 013 (2019)
44. B. Abi et al., Muon g-2 Collaboration, Phys. Rev. Lett. **126**, 141801 (2021)
45. T. Albahri et al., Muon g-2 Collaboration, Phys. Rev. D **103**, 072002 (2021)
46. T. Albahri et al., Muon g-2 Collaboration, Phys. Rev. A **103**, 042208 (2021)
47. G.W. Bennett et al., Muon g-2 Collaboration, Phys. Rev. D **73**, 072003 (2006)
48. J.L. Yang, T.F. Feng, Y.L. Yan, W. Li, S.M. Zhao, H.B. Zhang, Phys. Rev. D **99**(1), 015002 (2019)
49. J.L. Yang, H.B. Zhang, C.X. Liu, X.X. Dong, T.F. Feng, JHEP **08**, 086 (2021)
50. J.P. Lees et al., BaBar Collaboration, Phys. Rev. Lett. **109**, 191801 (2012)
51. J.P. Lees et al., BaBar Collaboration, Phys. Rev. D **86**, 052012 (2012)
52. T. Saito et al. [Belle Collaboration], Phys. Rev. D **91**(5), 052004 (2015)
53. J.L. Yang, T.F. Feng, S.M. Zhao, R.F. Zhu, X.Y. Yang, H.B. Zhang, Eur. Phys. J. C **78**(9), 714 (2018)